JCI The Journal of Clinical Investigation

SIRT1 inactivation switches reactive astrocytes to an anti-inflammatory phenotype in CNS autoimmunity

Weifeng Zhang, … , Abdolmohamad Rostami, Guang-Xian Zhang

J Clin Invest. 2022. https://doi.org/10.1172/JCI151803.

Research In-Press Preview **Autoimmunity** **Inflammation**

Graphical abstract

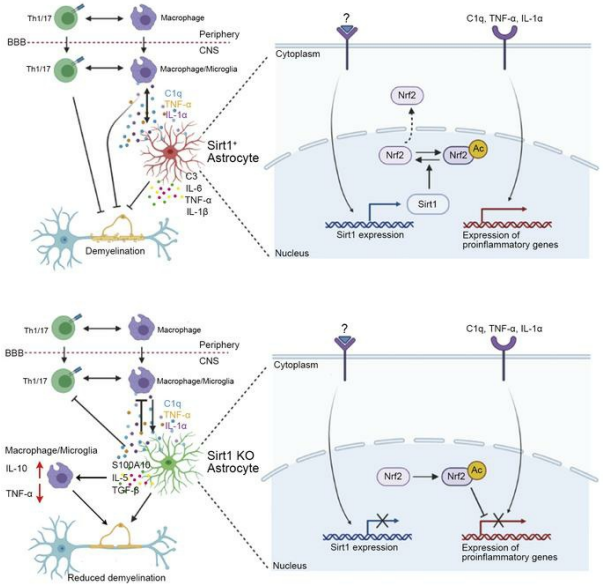

Find the latest version:

https://jci.me/151803/pdf

SIRT1 inactivation switches reactive astrocytes to an anti-inflammatory phenotype in CNS autoimmunity

Weifeng Zhang,[1,2] Dan Xiao,[1] Xing Li,[2] Yuan Zhang,[2] Javad Rasouli,[1] Giacomo Casella,[1] Alexandra Boehm,[1] Daniel Hwang,[1] Larissa Lumi Watanabe Ishikawa,[1] Rodolfo Thome,[1] Bogoljub Ciric,[1] Mark T. Curtis,[3] Abdolmohamad Rostami,[1*] and Guang-Xian Zhang[1*]

[1]Department of Neurology, Thomas Jefferson University, Philadelphia, Pennsylvania, USA.

[2]Department of Biochemistry, College of Life Sciences, Shaanxi Normal University, Xi'an, Shaanxi, China.

[3]Department of Pathology, Thomas Jefferson University, Philadelphia, Pennsylvania, USA.

Weifeng Zhang and Dan Xiao contributed equally to this work.

* Correspondence:

A.M. Rostami, Department of Neurology, Thomas Jefferson University, Philadelphia, Pennsylvania, USA. E-mail: a.m.rostami@jefferson.edu

Guang-Xian Zhang, Department of Neurology, Thomas Jefferson University, Philadelphia, Pennsylvania, USA. E-mail: Guang-Xian.Zhang@jefferson.edu

Abstract

Astrocytes are highly heterogenic in their phenotype and function, which contribute to CNS disease, repair and aging; however, the molecular mechanism of their functional states remains largely unknown. Here we show that activation of sirtuin 1 (SIRT1), a protein deacetylase, plays an important role in the detrimental actions of reactive astrocytes, whereas its inactivation endorsed these cells with anti-inflammatory functions that inhibited the production of proinflammatory mediators by myeloid cells/microglia and promoted the differentiation of oligodendrocyte progenitor cells. Mice with astrocyte-specific *Sirt1* knockout had suppressed progression of experimental autoimmune encephalomyelitis (EAE), an animal model of CNS inflammatory demyelinating diseases. Ongoing EAE was also suppressed when *Sirt1* expression in astrocytes was diminished by CRISPR/Cas vector, resulting in reduced demyelination, decreased numbers of T cells, and increased rate of IL-10-producing macrophages/microglia in the CNS, whereas peripheral immune response remained unaffected. Mechanistically, *Sirt1*$^{-/-}$ astrocytes expressed a range of nuclear factor erythroid-derived 2-like 2 (*Nfe2l2*) target genes, and *Nfe2l2* deficiency shifted the beneficial action of *Sirt1*$^{-/-}$ astrocytes to a detrimental one. These findings identify a novel approach for switching functional state of reactive astrocytes and facilitate the development of astrocyte-targeting therapies for inflammatory neurodegenerative diseases such as multiple sclerosis.

Keywords multiple sclerosis · EAE · astrocytes · Sirt1 · Nfe2l2

Introduction

Astrocytes, the most abundant cell type in the mammalian CNS, have been considered both an ally and enemy in the fight against CNS inflammation and restoration of neuronal function in multiple sclerosis (MS) (1-3). Astrocytes support neural transmission, sustain survival of neurons and other glia, and maintain the integrity of the blood-brain barrier (BBB) (1-3). Astrocyte scar formation aids, rather than prevents, CNS axon regeneration after spinal cord injury (4). Astrocytes also promote oligodendrocyte maturation and remyelination through production of neurotrophic factors, such as CNTF (5) and BDNF (6). Conversely, astrocytes are viewed as important non-professional antigen-presenting cells (APCs) and, during CNS inflammation, astrocytes around the MS lesion produce multiple pro-inflammatory mediators, including vasoactive molecules, chemoattractants, adhesion molecules, and cytokines that increase BBB permeability and promote lymphocyte recruitment, activation, and survival (1, 7). Reactive astrocytes undergo morphological, molecular, and functional remodeling in response to various pathological factors, and those toxic to neurons and oligodendrocytes have been classified as A1 astrocytes, while A2 astrocytes are likely neuroprotective, given their production of many neurotrophic factors (8). However, this binary classification may not well recapitulate the heterogeneity of astrocyte activation states (9). Astrocyte subsets have been more recently defined by their molecular signatures using more contemporary molecular techniques, e.g., single-cell RNA sequencing (scRNA-seq) and/or the function, which may reflect various sources of astrocyte heterogeneity (3). Understanding the mechanisms underlying astrocyte heterogeneity and plasticity may yield therapeutic approaches for switching astrocyte subsets from pathogenic to a beneficial one in neurological disorders such as MS.

Sirtuins (SIRTs), members of the class III histone/lysine deacetylase family, play critical roles in transcriptional regulation, cell cycling, replicative senescence, inflammation, and metabolism (10, 11). Among them, SIRT1 is expressed in many tissues and cell types and acts as an epigenetic regulator that

modulates the activity of several transcription factors important for immune function (12). While SIRT1 may have an anti-inflammatory role systemically (12, 13), likely via deacetylation of FOXP3 (14, 15), proinflammatory roles of SIRT1 have also been reported (16-18), whereby T cell- (19) or DC-specific (20) SIRT1 deletion protected mice from experimental autoimmune encephalomyelitis (EAE), an animal model of CNS inflammatory demyelinating disease. In the nervous system, SIRT1 plays a protective role in neurons (21-23) but an inhibitory role in oligodendrocyte progenitor cell (OPC) proliferation without affecting their differentiation (24, 25). The role of SIRT1 in astrocytes remains controversial, being either beneficial (22, 26, 27) or detrimental (25, 28, 29), whereas its role in astrocytes in MS/EAE remains unknown. We have in the present study defined the role of SIRT1 in the molecular profile and function of astrocytes and explored the potential of SIRT1 targeting in these cells as a CNS-specific therapy for MS.

Results

Inactivation of SIRT1 *promotes an anti-inflammatory phenotype in astrocytes in vitro.* To study the impact of SIRT1 on the phenotype and function of astrocytes, we first activated SIRT1 in primary astrocytes by resveratrol. Primary mouse astrocytes were prepared from C57BL/6 mice at P2-3 (30), with homogeneity of $GFAP^+$ cells >98% as determined by flow cytometry (Supplemental Figure 2). Activation with resveratrol alone did not affect gene expression of astrocytes; however, it significantly enhanced a cocktail (C1q, IL-1α and TNF)-induced expression of Complement component 3 (C3), a representative marker for neurotoxic astrocytes (8) (Figure 1A), together with proinflammatory cytokines IL-6, TNF, and IL-1β (Figure 1B). In contrast, S100A10, a marker likely for neuroprotective astrocytes (8), remained unchanged (Figure 1A).

Next, we tested whether the absence of SIRT1 impacts gene expression and function of astrocytes. Four sgRNAs targeting the exon4 of mouse *Sirt1* were synthesized, their knockout efficiencies tested in

the N2A-Cas9 cell line, and the most efficient sgRNA subcloned into a lentivirus carrying *Cre* and puromycin genes driven by EFS promoter (Figure 1C). Primary astrocytes were isolated from LSL-Cas9 transgenic mice carrying a Cas9-P2A-GFP cassette driven by CAG promoter, which was blocked by a floxed stop signal (Figure 1D). In this system, infection with the lentivirus carrying *Cre* gene can induce the expression of CAS9 in astrocytes, which, in combination with sgRNA expressed from lentivirus, cleaves the targeted sequence and leads to its knockout (31). *Sirt1* was knocked out in astrocytes with high efficiency, as shown by Western blot (Figure 1E). While lenti-sgScram-infected astrocytes treated with the cocktail developed an activated morphology, e.g., cellular hypertrophy, decreased fine processes (Figure 1F) with increased expression of glial fibrillary acidic protein (GFAP) (32) (Figure 1H), astrocytes with *Sirt1* knockout had a less activated morphology (Figure 1F). The RNA expression profile of astrocytes was substantially changed by *Sirt1* knockout as detected by microarray (Figure 1G). When further validated by real-time (RT)-PCR, reduced expression of cocktail-induced neurotoxic astrocyte markers and enhanced neuroprotective astrocyte markers were observed in *Sirt1*$^{-/-}$ astrocytes; however, there were no differences between *Sirt1*-sufficient vs. -deficient astrocytes in non-stimulated condition (Figure 1H). *Sirt1* knockout also reduced the expression of proinflammatory molecules NOS2, IL-6 and TNF and enhanced the expression of immunomodulatory molecules Arg1, IL-5 and TGF-β by cocktail-stimulated astrocytes (Figure 1I). Further, *Sirt1* knockout in astrocytes reduced their expression of chemokines CXCL5 and CCL20 (Figure 1J), which are important for CNS infiltration and proinflammatory functions of immune cells (33). These results suggest that *Sirt1* expression contributes to the development of neurotoxic/inflammatory state of astrocytes, and its inactivation promotes an anti-inflammatory one.

Reduced EAE progression and CNS inflammation in astrocyte-specific Sirt1$^{-/-}$ *mice.* To evaluate the role of SIRT1 in astrocytes in EAE, we induced EAE in mice lacking SIRT1 in GFAP^{+} cells (GFAP^{cre}*Sirt1*$^{fl/fl}$

mice). These mice initially developed EAE similar to the control *Sirt1*$^{fl/fl}$ mice, but then gradually recovered from the disease (Figure 2A). Histopathological analyses showed reduced immune-cell infiltration and demyelination (Figure 2B, D), with increased numbers of APC^{+} cells (newly matured oligodendrocytes) in the CNS lesions of GFAP^{cre}Sirt1$^{fl/fl}$ mice compared to the control mice (Figure 2C,E). Mononuclear cells (MNCs) isolated from the CNS were analyzed by flow cytometry. The total number of CD4^{+} T cells and myeloid cells was largely reduced in GFAP^{cre}Sirt1$^{fl/fl}$ mice (Figure 2F), with increased percentages of IL-10^{+} myeloid cells (CD11b^{+}CD45^{hi}) and microglia (CD11b^{+}CD45^{lo}) (Figure 2G,H). The frequencies of various CD4^{+} T-cell subtypes in the CNS were not different between these two mouse lines (Supplemental Figure 3A,B). Reduced numbers of C3^{+} astrocytes (Figure 2I,J) and increased numbers of S100A10^{+} ones (Figure 2K,L) were observed in the CNS lesions of GFAP^{cre}*Sirt1*$^{fl/fl}$ mice compared to *Sirt1*$^{fl/fl}$ mice. In contrast, no difference between these two groups was observed in the total numbers and subsets of monocytes and CD4^{+} T cells in their spleens (Supplemental Figure 4A-D) and draining lymph nodes (data not shown). These results show that SIRT1 in astrocytes plays an important role in EAE progression, possibly by promoting a neurotoxic/inflammatory astrocyte phenotype; further, its inactivation enhances anti-inflammatory astrocytes and suppresses CNS autoimmunity without affecting the peripheral immune response.

Sirt1$^{-/-}$ *astrocytes induced immunomodulatory microglia/macrophages and enhanced OPC differentiation.* We then determined the direct impact of astrocyte *Sirt1* on microglia/macrophages and oligodendrocytes in vitro. Given the reduced number of immune cells in the CNS of astrocyte-specific *Sirt1*$^{-/-}$ EAE mice (Figure 2F) and reduced CXCL5 and CCL20 secretion in *Sirt1*$^{-/-}$ astrocytes (Figure 1J), we tested the cause-effect relationship of these two phenomena in vitro. Thus, migration of splenocytes from mice with EAE toward astrocyte-conditioned medium (ACM) of cocktail-stimulated *Sirt1*$^{-/-}$ and WT astrocytes was tested

in a transwell system. Fewer total MNCs, $CD11b^+$ myeloid cells and $CD4^+$ T cells migrated toward the ACMs of *Sirt1*$^{-/-}$ astrocytes than toward ACMs of WT astrocytes, and this migration was reduced by neutralizing anti-CXCL5 and -CCL20 antibodies (Figure 3A).

Sirt1$^{-/-}$ mice had increased IL-10 secretion by microglia/myeloid cells in the CNS during EAE (as shown in Figure 2G,H). To test whether this is a direct consequence of Sirt1 knockout in astrocytes, primary microglia of WT mice were pre-activated with LPS, and *Sirt1*$^{-/-}$ or WT astrocytes were stimulated with the cocktail (C1q, IL-1α, TNF). These cells were then co-cultured and their expression of IL-10 and TNF was analyzed by flow cytometry. *Sirt1* knockout reduced the percentage of TNF^+ astrocytes and increased the percentage of IL-10^+ astrocytes (Figure 3B,C). Similarly, reduced percentage of TNF^+ microglia and increased percentage of IL-10^+ microglia were observed when they were co-cultured with *Sirt1*$^{-/-}$ astrocytes (Figure 3B,D). Given the enhanced expression of TGF-β by *Sirt1*$^{-/-}$ astrocytes (Figure 1I), which can influence the activation (34) and cytokine production of microglia (Supplemental Figure 5), we speculated that *Sirt1*$^{-/-}$ astrocytes could induce immunomodulatory microglia through increased TGF-β secretion. To test this, LPS-activated microglia were incubated with supernatants from cocktail-stimulated *Sirt1*$^{-/-}$ or WT astrocytes, with or without adding TGF-β-neutralizing antibody to the cultures. Whereas supernatants from *Sirt1*$^{-/-}$ astrocytes reduced TNF and increased IL-10 secretion by microglia, these effects were blocked by TGF-β neutralizing antibody (Figure 3E). Together, these results indicate that *Sirt1*$^{-/-}$ astrocytes directly affect the function of activated microglia, and immunomodulatory mediators such as TGF-β produced by these astrocytes play an important role in this effect.

We also analyzed the direct effect of ACMs from *Sirt1*$^{-/-}$ vs. WT astrocytes on the differentiation of OPCs. While OPCs cultured with ACMs from cocktail-stimulated WT astrocytes exhibited a low level of differentiation, as shown by <20% of $CNPase^+$ mature oligodendrocytes, this proportion was significantly increased (>40%) in those cultured with ACMs of *Sirt1*$^{-/-}$ astrocytes (Figure 3F, G). Taken together, these

results show that *Sirt1*$^{-/-}$ astrocytes can reduce immune cell migration and proinflammatory microglia polarization while enhancing OPC differentiation.

Sirt1$^{-/-}$ *astrocytes acquired anti-inflammatory function through NRF2 activation.* To define the mechanism underlying the role of *Sirt1* in astrocytes, we further analyzed the RNA expression profiles of *Sirt1*$^{-/-}$ vs. WT astrocytes. Among the altered genes shown in Figure 1G, *Sirt1*$^{-/-}$ astrocytes expressed increased levels of NQO1, xCT (*SLC7A11*), Srxn1, Gclc, and HO-1 (*HMOX1*), all of which are targets of the nuclear factor erythroid 2-related factor 2 (NRF2) transcription factor (35). Their expression was further confirmed by RT-PCR (Figure 4A); however, the expression of *Nfe2l2* gene remained unchanged (data not shown). NRF2 protein, encoded by *Nfe2l2* gene, is a transcription factor that has important anti-inflammatory and anti-oxidant functions (36). Given that acetylation of NRF2 is important for its function (37), we tested the impact of SIRT1 on NFR2 acetylation and found that *Sirt1*$^{-/-}$ astrocytes had greatly enhanced NRF2 acetylation (Figure 4B) localized in the nucleus (Figure 4C). To test the role of NRF2 in the SIRT1-mediated astrocyte function, *Nfe2l2* and *Sirt1* were simultaneously knocked out in primary WT astrocytes using the CRISPR/Cas technique (Figure 4D), and knockout efficacy was confirmed by Western blot (Figure 4E). Knockout of *Nfe2l2* abrogated the anti-inflammatory phenotype of *Sirt1*$^{-/-}$ astrocytes, as shown by increased expression of C3 and decreased expression of S100A10, IL-5 and TGF-β (Figure 4F). Thus, the NRF2 signaling pathway plays an important role in the anti-inflammatory transcriptional programs of *Sirt1*$^{-/-}$ astrocytes.

Adeno-associated virus (AAV)-CRISPR-mediated knockout of Sirt1 in astrocytes promoted recovery in ongoing EAE. To test whether astrocyte-specific *Sirt1* knockout can alleviate ongoing EAE, we generated AAV-transfer plasmid carrying a Cre gene driven by GFAP promoter and *Sirt1*-targeting sgRNA (Figure

5A). PHP.eB, a newly developed AAV serotype that efficiently transduces the CNS via systemic delivery in adult animals (38), was used to achieve astrocyte-specific knockout of *Sirt1* in the entire CNS (39). EAE was induced in LSL-Cas9 transgenic mice, and AAV was i.v. injected at day 15 post immunization (p.i.), when disease was still worsening. The efficacy of *Sirt1* knockout in astrocytes (GFP^+) was confirmed by immunostaining (Figure 5B). While both groups experienced a temporary reduction in disease severity, likely due to a non-specific effect of vector injection (40), an increased score was seen in mice after 10 days of control AAV injection. In contrast, disease severity remained suppressed in mice with astrocyte-specific knockout of *Sirt1* (Figure 5C), with greatly reduced infiltration of immune cells into the CNS (Figure 5D). AAV-sgSirt1 treatment increased numbers of IL-10^+ and reduced numbers of TNF^+ microglia/macrophages (Figure 5E,F), whereas the percentages of $CD4^+$ T-cell subtypes remained similar (Supplemental Figure 6). Furthermore, significantly increased percentages of $GFAP^+$ astrocytes colocalized with S100A10 were found in astrocytes of the AAV-sgSirt1-treated group (Figure 5G,H). The AAV-sgSirt1-treated group also upregulated expression of anti-inflammatory molecules in astrocytes, including chitinase 3 like 1 (CHI3L1) (41-43), sulfiredoxin-1 (SRXN1) (44), and TNF-related apoptosis-inducing ligand (TRAIL) (45) (Figure 6). In contrast, there was no difference in peripheral immune responses between these two groups (Supplemental Figure 7). These results demonstrate that CRISPR-mediated *Sirt1* knockout in astrocytes after disease onset exhibited an anti-inflammatory profile, which promotes recovery in ongoing EAE, thus having the potential for clinical application.

SIRT1 *is highly expressed in $C3^+$ astrocytes of MS patients.* $C3^+$ astrocytes have been found in the demyelinating plaques of MS patients, which may inhibit OPC proliferation/differentiation and induce oligodendrocytes (8). Here we tested the relationship of SIRT1 expression and C3/S100A10 in astrocytes of MS lesions. Brain slices from MS patients were co-stained for GFAP, SIRT1, and either C3 or S100A10;

normally-appearing white matter (NAWM) distant from the lesion served as control. A large number of $C3^+SIRT1^+GFAP^+$ cells were present in MS lesions (Figure 7A; lower panel), with nearly 71% of $C3^+$ astrocytes co-stained for SIRT1 (Figure 7B). However, only a few $S100A10^+SIRT1^+GFAP^+$ astrocytes were found in the lesions (Figure 7A lower panel), and only a few astrocytes were $SIRT1^+$, $C3^+$, or $S100A10^+$ in the NAWM area (Figure 7A upper panel). These findings demonstrate that *Sirt1* expression is closely associated with the proinflammatory/neurotoxic astrocytes of MS lesions.

Discussion

In the present study we found, as summarized in Supplemental Figure 8, that reactive astrocytes expressed a high level of SIRT1, exhibited proinflammatory/neurotoxic properties, and induced CNS demyelination. Inactivation of SIRT1 converted astrocytes into a glioprotective/anti-inflammatory phenotype in an NRF2-dependent manner. Genetic deletion of SIRT1 in astrocytes effectively inhibited EAE progression, and ongoing EAE was also suppressed by astrocyte-specific *Sirt1* knockout-CRISPR/Cas vector, without affecting peripheral immune responses. These findings define an approach for inducing glioprotective/anti-inflammatory astrocytes *in vitro* and *in vivo*, and provide a proof of concept for CNS-specific therapies for inflammatory neurodegenerative diseases such as MS.

It was initially thought that SIRT1 plays an anti-inflammatory role (12, 13), likely via deacetylation of FoxP3, the signature transcription factor of Tregs (14, 15); however, important proinflammatory actions of SIRT1 have been recently defined. For example, inhibition of SIRT1 expression in both mouse and human T cells resulted in increased numbers of $FoxP3^+$ Tregs (16-18). SIRT1 promotes autoimmunity by deacetylating RORγt, the signature transcription factor of Th17 cells, and T cell-specific *Sirt1* deletion or pharmacological inhibition of SIRT1 protects mice from EAE (19). $Sirt1^{-/-}$ DCs inhibited Th17 differentiation, and thereby attenuated the development of EAE (20). In the CNS, SIRT1 induces neural

progenitor cell differentiation into more astrocytes but fewer neurons (25); nevertheless, SIRT1 plays a protective role in neurons (21-23). In contrast, a detrimental role of SIRT1 in OPC/oligodendrocyte lineage has been identified. Neural stem cell (NSC)-specific knockout of *Sirt1* promotes differentiation of these cells to OPCs, which can normally mature into myelinating oligodendrocytes, and mice with NSC-specific knockout of *Sirt1* showed delayed EAE onset and enhanced remyelination (24). Similar results were obtained using a SIRT1 inhibitor (25). In a neonatal brain injury model, SIRT1 inhibition promotes OPC differentiation and neuroregeneration (46). Both beneficial and detrimental roles of SIRT1 expression have been described in astrocytes: For the former, overexpression of SIRT1 attenuates astrocyte activation in vitro, and improves neurobehavioral function after brain injury (22, 26). SIRT1 expression in astrocytes may have a neuroprotective effect through its anti-oxidative and anti-inflammatory functions (27). For the latter, astrocytes with decreased expression of PPARγ and SIRT1 protect neurons from Aβ1-42 peptide-induced neurotoxicity (28). Increased numbers of oligodendrocytes have also been observed in EAE lesions after treatment with resveratrol (25, 29), a SIRT1 activator with a large range of effects, including modulating signaling via aryl hydrocarbon receptor (AHR) (47), NF-κB, and other molecular pathways as well (48). Our study provides evidence for a detrimental role of SIRT1 in astrocytes, given that SIRT1 inactivation enables astrocytes to inhibit CNS inflammation and promote OPC differentiation, thus protecting the CNS from inflammation-induced myelin damage and enhancing disease recovery.

Our findings suggest that SIRT1 regulates the functional status of reactive astrocytes, at least in part, by inhibiting expression of signaling molecules (e.g., NQO-1, xCT, Srxn1, Gclc, HO-1) that are downstream of NRF2 (35). Indeed, SIRT1 exhibits diverse functions by deacetylating multiple targets, including FOXO, Ku70, p53, NF-κB, PGC-1α, RORγ, NRF2, and PPARγ (49). Among them, the transcription factor NRF2 controls cellular responses that limit oxidative stress and inflammation (50). Whole-body *Nfe2l2*-deficient mice develop severe EAE (51, 52), and *Nfe2l2*-deficient DCs induce

increased proportions of activated Th1/Th17 cells and fewer Treg cells (53). Further, NRF2 activity in astrocytes could be inhibited by pro-inflammatory cytokines IL-1β and TNF, and astrocyte-specific knockdown of *Nfe2l2* significantly enhanced EAE severity (54). We found that *Sirt1*$^{-/-}$ astrocytes had greatly enhanced NRF2 acetylation and its localization in the nucleus. *Sirt1*$^{-/-}$ astrocytes had a decreased expression of C3 and increased S100A10, IL-5 and TGF-β expression compared to *Sirt1*-sufficent control, and this profile was reversed by *Nfe2l2* knockout. Together with observations of others, our findings suggest that the deacetylation activity of SIRT1 suppresses the function of NRF2 in driving an anti-inflammatory program in astrocytes.

Among the molecules with altered expression in *Sirt1*$^{-/-}$ astrocytes in EAE mice, of particular interest is the upregulated expression of CHI3L1, SRXN1, and TRAIL. CHI3L1 expression has been associated with the immunomodulatory property of mesenchymal stem cells (55) and macrophages (43, 56). Expression of CHI3L1 in the CNS was predominantly associated with reactive astrocytes in the vicinity of inflammatory lesions, and CHI3L1-deficient mice showed more severe EAE and increased immune cell infiltrates and gliosis in the CNS (42). Here we showed enhanced CHI3L1 expression in *Sirt1*$^{-/-}$ astrocytes, which produced increased levels of IL-5, IL-10, and TGF-β, supporting a notion for anti-inflammatory function of CHI3L1 in reactive astrocytes in EAE. SRXN1, an endogenous antioxidant protein, exhibits neuroprotective effects, and loss of its expression in astrocytes may cause excessive activation of inflammatory responses and contribute to stress-induced neuronal death (44). These data suggest that upregulation of SRXN1 expression in astrocytes may, therefore, protect astrocyte-specific *Sirt1*$^{-/-}$ mice from EAE as shown in our observations. Further, a novel subset of lysosomal membrane glycoprotein 1 (LAMP1)$^{+}$TRAIL^{+} astrocytes has been recently identified, which limits CNS inflammation by inducing T-cell apoptosis through TRAIL-DR5 signaling (45, 57). Consistent with these important observations, our data showed enhanced TRAIL expression on astrocytes of astrocyte-specific *Sirt1*$^{-/-}$ EAE mice, with

reduced numbers of $CD4^+$ T cells in the CNS. Thus, in astrocyte-specific *Sirt1*$^{-/-}$ EAE mice, enhanced TRAIL expression on astrocytes may be an important mechanism underlying the reduced numbers of $CD4^+$ T cells and inflammatory demyelination of the CNS in astrocyte-specific *Sirt1*$^{-/-}$ EAE mice.

Considerable progress has been made in immunomodulatory therapies that reduce the severity and progression of MS; however, existing therapies mainly target the peripheral immune system and have side effects such as suppression of systemic immune responses (58, 59). An approach to overcome this weakness could be targeting only the CNS, and astrocytes could be an ideal target for this purpose. Indeed, in astrocytes, blocking signaling of proinflammatory molecules, such as IL-17, ameliorated EAE (60, 61). EAE was also suppressed by inactivation of other proinflammatory molecules in astrocytes, including B4GALT6 (62), inositol-requiring enzyme-1a (IRE1a), X-box binding protein 1 (XBP1) (63), Ugcg (64), MAFG, MAT2a and GM-CSF signaling (54); whereas CNS autoimmunity worsened by inactivation of immunomodulatory molecules in astrocytes, e.g., AHR (65, 66) or NRF2 (54). Consistent with these observations, in the present study we verified the potential of SIRT1 inactivation in astrocytes as a method for the therapy of ongoing disease by using the CRISPR/Cas technique.

AAV has been safely used in clinical trials for neurological disorders, e.g., Parkinson's disease (67). Using the CAS13-mediated RNA targeting technique developed in recent years to silence *Sirt1* expression in astrocytes could provide a safe and feasible method for clinical use (68, 69). Furthermore, CNS-specific treatment directly targets the inflammatory demyelination process in the lesion foci and could thus be more effective than systemic treatments. For example, while systemic administration of IL-10 failed to suppress EAE, delivery of cells that expressed IL-10 into the CNS had a significant therapeutic effect (70). Together, our findings demonstrate that *Sirt1* expression in reactive astrocytes plays a pathogenic role in inflammatory demyelination, and its inactivation in these cells may represent a novel strategy for CNS-specific EAE/MS therapy.

Methods

Animals. C57BL/6J (stock no. 000664), GFAP-Cre (stock no. 024098), Sirt1$^{fl/fl}$ (stock no. 029603), and LSL-Cas9 (stock no. 026175) mice were purchased from the Jackson Laboratory (Bar Harbor). Astrocyte-specific *Sirt1*$^{-/-}$ mice were generated by crossing GFAP-Cre and Sirt1$^{fl/fl}$ mice, and deletion of *Sirt1* in astrocytes was verified by PCR and Western blot (data not shown). All animals were kept in a pathogen-free facility at Thomas Jefferson University. All experiments were carried out in accordance with guidelines prescribed by the Institutional Animal Care and Use Committee (IACUC) of Thomas Jefferson University.

Cell lines. N2A-Cas9 cell line was purchased from Genecopoeia (Rockville) and grown in DMEM containing 10% FBS. HEK293 cells were also cultured in DMEM containing 10% FBS (Thermo Scientific). Cells were maintained at 37^{o}C in 5% CO_2 atmosphere.

Plasmids. LentiCRISPR v2 and AAV:ITR-U6-sgRNA(backbone)-pCBh-Cre-WPRE-hGHpA-ITR were a gift from Dr. Feng Zhang (MIT). For construction of pLenti-sgRNA(backbone)-EFS-Cre-P2A-Puro, the *Cas9* sequence in lentiCRISPR v2 was replaced by a *Cre* gene sequence (Supplemental Figure 1A). Single guide RNAs (sgRNAs) targeting mouse *Sirt1* or *Nfe2l2* were subcloned into pLenti-sgRNA(backbone)-EFS-Cre-P2A-Puro through *BsmB*; the obtained plasmids were named pLenti-EFS-Cre-P2A-Puro-sgSirt1 or pLenti-EFS-Cre-P2A-Puro-sgNfe2l2. Scramble sgRNA (sgScram) was also cloned into pLenti-EFS-Cre-P2A-Puro as control.

To knockout *Sirt1* in astrocytes of adult mice, GFAP promoter was amplified from pLenti-Gfap-eGFP-mir30-shAct1 vector (61) and cloned into AAV:ITR-U6-sgRNA(backbone)-pCBh-Cre-WPRE-hGHpA-ITR to replace CBh promoter; the obtained plasmid was named pAAV-sgRNA(backbone)-GFAPp-Cre (Supplemental Figure 1B). The U6-sgSirt1 or U6-sgScram cassette was cleaved from pLenti-EFS-Cre-

P2A-Puro-sgSirt1 or pLenti-EFS-Cre-P2A-Puro-sgScram and cloned into pAAV-sgRNA(backbone)-GFAPp-Cre; the resulting plasmid was named pAAV-sgSirt1-GFAPp-Cre or pAAV-sgScram-GFAPp-Cre.

pAdδF6 was a gift from James M. Wilson (University of Pennsylvania); pUCmini-iCAP-PHP.eB was a gift from Viviana Gradinaru (California Institute of Technology); psPAX2 and pMD2.G were a gift from Didier Trono (EPFL). All of the primers used are listed in Supplementary Table 1.

sgRNA design and screen. sgRNAs targeting *Sirt1* and *Nfe2l2* were designed using https://www.benchling.com/crispr/; corresponding primers were synthesized by Integrated DNA Technologies, Inc. (Coralville, Iowa, USA). Primers were annealed and ligated into pLenti-EFS-Cre-P2A-Puro, sgRNAs activity was analyzed in N2A-Cas9 cell line. For sgRNAs activity analysis, N2A-Cas9 cells were seeded in a 24-well plate at 1×10^5 cells per well, and, on the following day, were transfected with a mixture containing 0.5 μg sgRNA-carrying plasmid and 1 μl Lipofectamine™ 2000 (Thermo Scientific). Medium was changed on the next day, and cells collected 48 h after transfection. Knockout efficiency was analyzed by Western blot. All of the primers used are listed in Supplementary Table 1.

Virus packaging and purification. The lentivirus particles were generated by transfecting 293T cells with transfer plasmid, psPAX2 and pMD2.G, using PEI-MAX (Polysciences). Supernatant was collected at 30 h and 48 h after transfection, filtered through 0.45-μm PVDF filter, and concentrated overnight with 40% PEG-10000 (Sigma).

The AAV particles were generated as reported by Chan et al. (38). Low-passaged 293T cells were transfected with transfer plasmid, pUCmini-iCAP-PHP.eB, and pAdDeltaF6, using PEI-MAX (Polysciences); viral particles were collected at 72 h after transfection from the medium and 120 h after transfection from cells and the medium. The supernatant was concentrated with 40% PEG-8000 (Thermo Scientific) and combined with cell pellets for processing. The cell pellets were suspended in 500 mM NaCl, 40 mM Tris, 2.5 mM $MgCl_2$, pH 8, and 100 U/mL of salt-activated nuclease (SAN) (Sigma) at 37°C for 1

h. Afterwards, the cell lysates were clarified by centrifugation at 2,000 g and then purified using iodixanol (Sigma) step gradients (15%, 25%, 40%, and 60%) (71). Viruses were concentrated using Amicon filters (Millipore) and formulated in sterile phosphate-buffered saline (PBS) with 0.001% Pluronic-F68 (Thermo Scientific). Virus titers were measured by determining the number of DNAse I-resistant vg using qPCR with a linearized genome plasmid as a standard (72).

EAE induction and treatment. Female GFAP^{cre}*Sirt1*$^{fl/fl}$ and *Sirt1*$^{fl/fl}$ mice, 8–10 weeks of age, were used for EAE induction. Mice were immunized subcutaneously at two sites on the back with 200 μg $MOG_{35–55}$ peptide (GenScript) emulsified in CFA (BD Bioscience) supplemented with 4 mg/ml Mycobacterium tuberculosis H37Ra (BD Bioscience); 200 ng pertussis toxin (Sigma) was injected intraperitoneally into each mouse on days 0 and 2 p.i. All mice were monitored for weights and clinical signs daily until 25 or 30 days post induction of EAE. Mice were euthanized if they showed a 20% loss in maximum body weight. Gel food was supplied at the onset of EAE disease. Clinical scores were recorded on the following scale: 0, no clinical signs; 1, limp tail; 2, limp tail with weak/partially paralyzed hind legs; 3, limp tail with completely paralyzed hind legs; 4, tetraplegia; 5, moribund.

Astrocyte-specific Sirt1 knockout during ongoing EAE. AAV PHP.eB at 2×10^{11} vg was diluted in 200 μl PBS with 0.001% Pluronic-F68, and then injected through the tail vein into LSL-Cas9 mice at day 15 p.i. Two weeks after injection, mice were sacrificed and knockout efficiency was analyzed by immunostaining.

Isolation of immune cells from the CNS and spleen. Brains and spinal cords from naive and EAE mice were removed, minced, and enzymatically dissociated with Liberase TL (Roche) for 30 min at 37ºC. Liberase was neutralized by DMEM supplemented with 10% FBS; cells were then passed through a 70 μm cell strainer and centrifuged, resuspended in 30% Percoll (Sigma), overlaid onto 70% Percoll, and centrifuged at 2000 rpm at 4ºC for 20 min with slow acceleration and deceleration settings. Immune cells

were collected from the 30-70% interphase. Spleens of naïve or EAE mice were dispersed into single cell level by passing through a 40 μm cell strainer and erythrocytes were removed using RBC Lysis Buffer (Biolegend). For flow cytometry analysis, cells were seeded in a 24-well plate at a concentration of 1×10^6 cells per well, treated with phorbol 12-myristate-13-acetate (PMA; 50 ng/ml; Sigma), Ionomycin (500 ng/ml; Sigma), and BD GolgiPlug™ (1 μg/ml; BD Bioscience) for 4 h, then analyzed by flow cytometry.

Immune cell migration assay. The immune cells were isolated from the spleens of naïve or EAE mice and seeded in the upper chamber of a 24-well cell culture insert with 5-μm pore-size (Corning Inc.). The lower chamber was filled with culture supernatant of cocktail stimulated *Sirt1*-knockout or WT astrocytes (ACMs). Migrating immune cells were quantified in the lower chamber after 2 h by cell counting and flow cytometry.

Flow cytometry. Cells were first stained with surface antibody at 4°C for 20 min, fixed by Fixation Medium (Medium A) (Thermo Scientific), washed, and then incubated with intracellular antibody dissolved in Permeabilization Medium (Medium B) (Thermo Scientific) at 4°C overnight. Antibodies used in this study were: APC anti-mouse CD45 (BD Bioscience, clone 30-F11), P-blue anti-mouse CD4 (BD Bioscience, clone RM4-5), PE anti-mouse IL-17 (BD Bioscience, clone TC11-18H10), BV711 anti-mouse IFN-γ (BD Bioscience, clone XMG1.2), AF488 anti-mouse Foxp3 (eBioscience, clone FJK-16s), PerCP-Cy5.5 anti-mouse CD11b (BD Bioscience, clone M1/70), PE-Cy7 anti-mouse IL-4 (BD Bioscience, clone 11b11), BV605 anti-mouse IL-10 (Biolegend, Clone JES5-16E3), and PE-Dazzle594 anti-TNF (Biolegend clone, MP6-XT22). Compensation was performed with UltraComp eBeads™ (Thermo Scientific, 01-2222-42).

Isolation of primary astrocytes. Primary astrocytes were isolated as previously reported (54). Cerebral cortices of mice aged P0-P3 were dissected, carefully stripped of their meninges, and digested with Liberase TL (Roche) (2 U/ml) at 37°C for 15 min. Liberase was neutralized by DMEM supplemented with

10% FBS, and cells were passed through a 70 μm cell strainer. The cell suspension was then cultured with DMEM containing 10% FBS at 37°C in humidified 5% CO_2, 95% air on T-175 cell culture flasks for 7-10 days until confluency was reached. Medium was replaced every 4–5 days. After the cells reached confluency, microglia and oligodendrocytes were removed by shaking the glia culture at 260 rpm at 37ºC overnight and washing extensively with PBS; the remaining attached cells were astrocytes with purity greater than 98% (Supplemental Figure 2). It has been shown that primary astrocytes cultured with serum-containing medium may induce a reactive phenotype in astrocytes (73). While FBS containing medium was used during astrocyte isolation to enhance their viability, we cultured these cells under serum-free conditions. These cells did not express reactive astrocyte markers in non-stimulation culture condition (as shown in Figure 1H), indicating a minor impact of FBS during astrocyte isolation, while culturing them in a serum-free condition.

Astrocyte treatment in vitro. For SIRT1 activation, 5×10^5 primary astrocytes were seeded in a 6-well plate in astrocyte serum-free medium. The following day, cells were incubated with 10 μg/ml Resveratrol (Sigma) for 24 h, and then treated with cytokine cocktail (C1q, IL-1α, TNF) for an additional 24 h, as previously reported (8).

For *Sirt1* knockout analysis, 5×10^5 *Sirt1* knockout or WT astrocytes were seeded in a 6-well plate in astrocyte serum-free medium. The following day, cells were treated with cytokine cocktail for 24 h, as previously reported (8).

For RT-PCR and ELISA analysis, the cells and supernatants were collected immediately after cocktail stimulation. For ACM collection, cells were, after cocktail stimulation, washed with PBS and incubated with fresh, serum-free medium for an additional 24 h. The supernatants were collected, filtered through 0.45 μm filter and kept at 4ºC until use.

Microarray. Primary astrocytes isolated from p2-3 LSL-Cas9 pups were infected with sgSirt1 or sgScram carrying lentivirus, and then selected with 4 μg/ml puromycin for 3 days. Cells were stimulated with cocktail (C1q, IL-1α, TNF) for an additional 24 hours and then collected for microarray analysis. Four samples, namely sg-Scarm-1, sg-Scarm-2, sg-Sirt1-1 and sg-Sirt1-2, were analyzed at the Cancer Genomics and Bioinformatics Resource (CGBR), Thomas Jefferson University. The data have been deposited in NCBI GEO under accession number (GSE212924).

Sirt1 or Nfe2l2 knockout in vitro. For *Sirt1* or *Nfe2l2* knockout, primary mouse astrocytes isolated from LSL-Cas9 mice were incubated for 24 h with *Sirt1* or *Nfe2l2* sgRNA carrying lentiviruses and 8 μg/ml polybrene (Millipore), after which the medium was changed. Cells were, 48 h after infection, selected with 4 μg/ml puromycin for 3 days. Knockout of *Sirt1* or *Nfe2l2* was verified by Western blot.

Microglia isolation, culture, and treatment in vitro. Brains from mouse pups (P7) were dissociated into single-cell suspension using the Neural Tissue Dissociation Kit (P) (Miltenyi) according to the manufacturer's protocol. Microglia was isolated from single-cell suspension using CD11b microbeads (Miltenyi) and cultured in DMEM/F12 with 10% FBS (74). Cells were stimulated by LPS (100 ng/ml) for 18 h, then washed and incubated with fresh medium containing TGF-β or ACMs.

OPC isolation and differentiation in vitro. Brains from mouse pups (P2-3) were dissociated into single-cell suspension using the Neural Tissue Dissociation Kit (P) (Miltenyi) according to the manufacturer's protocol. OPCs were isolated from single-cell suspension using CD140a microbeads (Miltenyi). OPC proliferation and differentiation media were prepared as previously described with some modifications (75). OPC proliferation medium comprised DMEM/F12 (Thermo Scientific), N2 Supplement (Thermo Scientific), B27 Supplement (Thermo Scientific), bFGF 20 ng/ml (Peprotech), and PDGF-AA 20 ng/ml (Peprotech). bFGF and PDGF-AA were removed and T3 (Sigma) was added in OPC differentiation medium. 2×10^3 OPCs were seeded on poly-D-lysine (Sigma) and laminin (Sigma) coated

pre-sterilized glass coverslips (Carolina) in a 24-well plate. Cells were kept in OPC-proliferation medium for 2 days, and then in medium consisting of OPC differentiation medium and ACM at a ratio of 1:1 for 8 days. Medium was half-changed every 2-3 days. Differentiation was analyzed by cell immunostaining.

Immunohistochemistry. Both mice and human tissues were fixed with 4% paraformaldehyde, embedded in paraffin, and cut into 4 μm sections. Paraffin sections were stained with hematoxylin and eosin (H&E) for assessment of inflammation and Luxol fast blue (LFB) for demyelination. For immunofluorescence stain, paraffin sections were deparaffinized, washed in running water, and treated with heat retrieval solution (Biocare). The slides were then cooled in running water, washed with TBS, permeated by TBS with 0.2% Triton X-100 and blocked in TBS with 10% horse serum and 1% BSA for I h. The primary antibodies were then incubated in TBS with 1% horse serum and 1% BSA at 4ºC overnight. The following day, the slides were washed three times by TBS with 0.025% Triton X-100, incubated with secondary antibody (Jackson) in TBS with 1% horse serum and 1% BSA at room temperature for 1 h. Frozen tissues were cut into 10 μm sections in our lab. Frozen sections were air dried, rehydrated in TBS, permeated by TBS with 0.2% Triton X-100, and blocked in TBS with 10% horse serum and 1% BSA for 30 min. The primary and secondary antibodies were then incubated as above. Cells seeded on glass coverslip were washed with TBS, fixed by 4% paraformaldehyde, and permeated by TBS with 0.2% Triton X-100. Cells were then incubated with primary antibody in TBS with 10% horse serum and 1% BSA for 1 h at room temperature, washed in TBS three times, and incubated with secondary antibody in TBS with 1% horse serum and 1% BSA for 30 min at room temperature. Finally, all of the sections and coverslips were washed and mounted in Prolong Gold antifade reagent with DAPI (Thermo Scientific). Imaging was performed using a Nikon A1R microscope and Nikon NIS Elements acquisition and analysis software. Images were processed and analyzed by ImageJ.

The antibodies used were: goat anti-GFAP (mouse & human) (Abcam, ab53554), rabbit anti-GFAP (mouse & human) (CST, 12389, clone D1F4Q), rabbit anti-mSIRT1 (Abcam, ab12193), mouse anti-mCNP (Abcam, ab6319, clone 11-5B), mouse anti-mAPC (EMD Millipore, OP80, clone CC1), goat anti-C3d (mouse & human) (R&D, AF2655), rabbit anti-S100A10 (mouse & human) (Abcam, MA5-15326, 4E7E10), rabbit anti-SRXN1 (MyBioSource, MBS716745), rabbit anti-CHI3L1 (Abcam, ab255297, EPR19078-157), rabbit anti-TRAIL (Abcam, ab231265), chicken anti-GFP (Abcam, ab13970), rabbit anti-mNRF2 (Novus Biologicals, NBP1-32822), and mouse anti-hSIRT1 (EMD Millipore 04-1557; clone 10E4).

NRF2 acetylation detection. 3×10^6 sgSirt1- or sgScram-treated astrocytes were seeded in a 100 mm dish, stimulated with cocktail for 24 h, and then collected and lysed with 300 µl 1× cell lysis buffer (CST). 200 µl of cell lysate were incubated with 2 µl anti-NRF2 antibody (Novus Biologicals, NBP1-32822) at 4ºC overnight, then incubated with 20 µl protein-A (Thermo Scientific) at 4ºC for 3 h. The beads were washed with 1× cell lysis buffer three times, centrifuged, and 50 µl of 2 × loading buffer was added. The mixture was boiled at 95°C for 5 min to denature the proteins and to dissociate them from the protein-A beads; then they were centrifuged, and the supernatants were separated by SDS-PAGE and detected by purified anti-acetylated lysine antibody (Biolegend, 623402, clone 15G10).

Western blot. 1×10^6 WT, *Sirt1*-knockout or *Nfe2l2*-knockout astrocytes were lysed in 200 µl RIPA lysis buffer (Thermo Scientific) containing proteases inhibitors (Sigma). Cells were incubated on ice for 30 min, and sonicated for 10 s, with the cells being kept on ice during sonication. The cell lysate was centrifuged for 10 min at 4°C. Protein concentrations were determined using the BCA Protein Assay Kit (Thermo Scientific). Protein lysates were diluted in SDS-PAGE sample buffer, separated on Novex™ 4-12% Tris-Glycine gel (Thermo Scientific), and analyzed by Western blot using rabbit anti-*Sirt1* polyclonal

antibody (Abcam) or anti-NRF2 antibody (Invitrogen). GAPDH was detected by rabbit anti-GAPDH monoclonal antibody (CST) and used as loading control.

RT-PCR. RNA was extracted using RNeasy Mini Kit (Qiagen). cDNA was reverse-transcribed using QuantiTect Rev. Transcription Kit (Qiagen). Gene expression was quantified by qPCR using SYBR Green Mix (Thermo Scientific). The expression of each gene was normalized to GAPDH and then to the control group. All of the primers used here are listed in Supplementary Table 1.

MS tissues. Brain tissue was obtained from untreated individuals with clinically diagnosed and neuropathologically confirmed MS (Rocky Mountain MS Center Tissue Bank, Aurora, CO). All MS individuals, or their next of kin, had given informed consent for an autopsy and use of their brain tissue for research purposes. All the procedures were performed in accordance with local Institutional Review Board guidelines.

Statistics. Statistical analyses were performed with Prism software (GraphPad). Unpaired two-tailed t-test was used for comparison of two groups. One-way ANOVA was applied for comparison of more than two groups. Two-way repeated measures ANOVA was used for comparisons of clinical scores. P values of <0.05 were considered significant. All error bars represent SEM or SD as noted in the individual figure legends. Unless otherwise stated, ≥ 3 independent experiments were used for all assays, and displayed figures are representative.

Study approval. All animal studies were approved by the IACUC of the Thomas Jefferson University -approval S25801.

Author contributions

W.Z., D.X., and G.X.Z. conceived and designed the experiments, analyzed data, and wrote the manuscript. W.Z. and D.X. carried out the experiments. X.L. and Y.Z. helped with the experimental design

and statistical analysis. J.R. performed flow cytometry experiments. G.C. helped in the OPC differentiation experiments. A.B helped in some of the *in vitro* experiments. D.H, L.L., W.I., and R.T. helped with EAE experiments and revised the manuscript. M.C. helped with evaluating immunohistological results and revised the manuscript. B.C. and A.R. co-supervised the study and wrote the paper. All authors read and approved the final manuscript.

Acknowledgments

This work was supported by NIH grants NS099594 and AI135601; W.Z. and D.X. were partly supported by Chinese National Natural Science Foundation grant 31601086. We thank Ms. Katherine Regan and Ms. Pamela Walter for editorial assistance. We also thank Dr. Sandar Addya and Dr. Mobin Saddiqui for helping microarray data deposit.

Conflict of interest

The authors have declared that no conflict of interest exists.

References

1. Brambilla R. The contribution of astrocytes to the neuroinflammatory response in multiple sclerosis and experimental autoimmune encephalomyelitis. *Acta Neuropathol.* 2019;137(5):757-83.
2. Giovannoni F, Quintana FJ. The Role of Astrocytes in CNS Inflammation. *Trends Immunol.* 2020;41(9):805-19.
3. Lee HG, et al. Function and therapeutic value of astrocytes in neurological diseases. *Nat Rev Drug Discov.* 2022;21(5):339-58.
4. Anderson MA, et al. Astrocyte scar formation aids central nervous system axon regeneration. *Nature.* 2016;532(7598):195-200.
5. Nash B, et al. Functional duality of astrocytes in myelination. *J Neurosci.* 2011;31(37):13028-38.
6. Fulmer CG, et al. Astrocyte-derived BDNF supports myelin protein synthesis after cuprizone-induced demyelination. *J Neurosci.* 2014;34(24):8186-96.
7. Pitt D, Ponath G. Astrocytes play a crucial role in the formation and evolution of MS lesions - Yes. *Mult Scler.* 2019;25(1):15-7.
8. Liddelow SA, et al. Neurotoxic reactive astrocytes are induced by activated microglia. *Nature.* 2017;541(7638):481-7.
9. Escartin C, et al. Reactive astrocyte nomenclature, definitions, and future directions. *Nat Neurosci.* 2021;24(3):312-25.
10. Chang HC, Guarente L. SIRT1 and other sirtuins in metabolism. *Trends Endocrinol Metab.* 2014;25(3):138-45.
11. Haigis MC, Sinclair DA. Mammalian sirtuins: biological insights and disease relevance. *Annu Rev Pathol.* 2010;5:253-95.
12. Zhang J, et al. The type III histone deacetylase Sirt1 is essential for maintenance of T cell tolerance in mice. *J Clin Invest.* 2009;119(10):3048-58.
13. Gao B, et al. Analysis of sirtuin 1 expression reveals a molecular explanation of IL-2-mediated reversal of T-cell tolerance. *Proc Natl Acad Sci U S A.* 2012;109(3):899-904.

14. Kwon HS, et al. Three novel acetylation sites in the Foxp3 transcription factor regulate the suppressive activity of regulatory T cells. *J Immunol.* 2012;188(6):2712-21.

15. Liu G, et al. Dendritic cell SIRT1-HIF1alpha axis programs the differentiation of CD4+ T cells through IL-12 and TGF-beta1. *Proc Natl Acad Sci U S A.* 2015;112(9):E957-65.

16. van Loosdregt J, et al. Regulation of Treg functionality by acetylation-mediated Foxp3 protein stabilization. *Blood.* 2010;115(5):965-74.

17. Beier UH, et al. Histone/protein deacetylases control Foxp3 expression and the heat shock response of T-regulatory cells. *Curr Opin Immunol.* 2011;23(5):670-8.

18. Daenthanasanmak A, et al. Targeting Sirt-1 controls GVHD by inhibiting T-cell allo-response and promoting Treg stability in mice. *Blood.* 2019;133(3):266-79.

19. Lim HW, et al. SIRT1 deacetylates RORgammat and enhances Th17 cell generation. *J Exp Med.* 2015;212(5):607-17.

20. Yang H, et al. Histone deacetylase sirtuin 1 deacetylates IRF1 protein and programs dendritic cells to control Th17 protein differentiation during autoimmune inflammation. *J Biol Chem.* 2013;288(52):37256-66.

21. Di Sante G, et al. Sirt1-deficient mice have hypogonadotropic hypogonadism due to defective GnRH neuronal migration. *Mol Endocrinol.* 2015;29(2):200-12.

22. Zhang Z, et al. Sirt1 improves functional recovery by regulating autophagy of astrocyte and neuron after brain injury. *Brain Res Bull.* 2019;150:42-9.

23. Pallas M, et al. Modulation of sirtuins: new targets for antiageing. *Recent Pat CNS Drug Discov.* 2008;3(1):61-9.

24. Rafalski VA, et al. Expansion of oligodendrocyte progenitor cells following SIRT1 inactivation in the adult brain. *Nat Cell Biol.* 2013;15(6):614-24.

25. Prozorovski T, et al. Regulation of sirtuin expression in autoimmune neuroinflammation: Induction of SIRT1 in oligodendrocyte progenitor cells. *Neurosci Lett.* 2019;704:116-25.

26. Li D, et al. Interactions between Sirt1 and MAPKs regulate astrocyte activation induced by brain injury in vitro and in vivo. *J Neuroinflammation.* 2017;14(1):67.

27. Cheng Y, et al. Sirtuin 1 attenuates oxidative stress via upregulation of superoxide dismutase 2 and catalase in astrocytes. *J Neuroimmunol.* 2014;269(1-2):38-43.

28. Aguirre-Rueda D, et al. Astrocytes protect neurons from Abeta1-42 peptide-induced neurotoxicity increasing TFAM and PGC-1 and decreasing PPAR-gamma and SIRT-1. *Int J Med Sci.* 2015;12(1):48-56.

29. Prozorovski T, et al. Sirt1 contributes critically to the redox-dependent fate of neural progenitors. *Nat Cell Biol.* 2008;10(4):385-94.

30. Chao CC, et al. Metabolic Control of Astrocyte Pathogenic Activity via cPLA2-MAVS. *Cell.* 2019;179(7):1483-1498.e22.

31. Platt RJ, et al. CRISPR-Cas9 knockin mice for genome editing and cancer modeling. *Cell.* 2014;159(2):440-55.

32. Zhou B, et al. Astrocyte morphology: Diversity, plasticity, and role in neurological diseases. *CNS Neurosci Ther.* 2019;25(6):665-73.

33. Lepennetier G, et al. Cytokine and immune cell profiling in the cerebrospinal fluid of patients with neuro-inflammatory diseases. *J Neuroinflammation.* 2019;16(1):219.

34. Noh MY, et al. Mesenchymal Stem Cells Modulate the Functional Properties of Microglia via TGF-beta Secretion. *Stem Cells Transl Med.* 2016;5(11):1538-49.

35. Hayes JD, Dinkova-Kostova AT. The Nrf2 regulatory network provides an interface between redox and intermediary metabolism. *Trends Biochem Sci.* 2014;39(4):199-218.

36. Tu W, et al. The Anti-Inflammatory and Anti-Oxidant Mechanisms of the Keap1/Nrf2/ARE Signaling Pathway in Chronic Diseases. *Aging Dis.* 2019;10(3):637-51.

37. Kawai Y, et al. Acetylation-deacetylation of the transcription factor Nrf2 (nuclear factor erythroid 2-related factor 2) regulates its transcriptional activity and nucleocytoplasmic localization. *J Biol Chem.* 2011;286(9):7629-40.

38. Chan KY, et al. Engineered AAVs for efficient noninvasive gene delivery to the central and peripheral nervous systems. *Nat Neurosci.* 2017;20(8):1172-9.

39. Xiao D, et al. CRISPR-mediated rapid generation of neural cell-specific knockout mice facilitates research in neurophysiology and pathology. *Molecular Therapy - Methods & Clinical Development.* 2021;20:755-64.

40. Keeler GD, et al. Gene Therapy-Induced Antigen-Specific Tregs Inhibit Neuro-inflammation and Reverse Disease in a Mouse Model of Multiple Sclerosis. *Mol Ther.* 2018;26(1):173-83.

41. Henrik Heiland D, et al. Tumor-associated reactive astrocytes aid the evolution of immunosuppressive environment in glioblastoma. *Nat Commun.* 2019;10(1):2541.

42. Bonneh-Barkay D, et al. Exacerbation of experimental autoimmune encephalomyelitis in the absence of breast regression protein 39/chitinase 3-like 1. *J Neuropathol Exp Neurol.* 2012;71(11):948-58.

43. He CH, et al. Chitinase 3-like 1 regulates cellular and tissue responses via IL-13 receptor alpha2. *Cell Rep.* 2013;4(4):830-41.

44. Yu S, et al. Sulfiredoxin-1 protects primary cultured astrocytes from ischemia-induced damage. *Neurochem Int.* 2015;82:19-27.

45. Sanmarco LM, et al. Gut-licensed IFNgamma(+) NK cells drive LAMP1(+)TRAIL(+) anti-inflammatory astrocytes. *Nature.* 2021;590(7846):473-9.

46. Jablonska B, et al. Sirt1 regulates glial progenitor proliferation and regeneration in white matter after neonatal brain injury. *Nat Commun.* 2016;7:13866.

47. Assefa EG, et al. Role of Resveratrol on Indoxyl Sulfate-Induced Endothelial Hyperpermeability via Aryl Hydrocarbon Receptor (AHR)/Src-Dependent Pathway. *Oxid Med Cell Longev.* 2019;2019:5847040.

48. Alesci A, et al. Resveratrol and Immune Cells: A Link to Improve Human Health. *Molecules.* 2022;27(2).

49. Ren Z, et al. The role of different SIRT1-mediated signaling pathways in toxic injury. *Cell Mol Biol Lett.* 2019;24:36.

50. Cuadrado A, et al. Therapeutic targeting of the NRF2 and KEAP1 partnership in chronic diseases. *Nat Rev Drug Discov.* 2019;18(4):295-317.

51. Johnson DA, et al. The absence of the pro-antioxidant transcription factor Nrf2 exacerbates experimental autoimmune encephalomyelitis. *Toxicol Sci.* 2010;114(2):237-46.

52. Bernstein AI, Miller GW. Oxidative signaling in experimental autoimmune encephalomyelitis. *Toxicol Sci.* 2010;114(2):159-61.

53. Hammer A, et al. Role of Nuclear Factor (Erythroid-Derived 2)-Like 2 Signaling for Effects of Fumaric Acid Esters on Dendritic Cells. *Front Immunol.* 2017;8:1922.

54. Wheeler MA, et al. MAFG-driven astrocytes promote CNS inflammation. *Nature.* 2020;578(7796):593-9.

55. Liu Q, et al. Mesenchymal stem cells alleviate experimental immune-mediated liver injury via chitinase 3-like protein 1-mediated T cell suppression. *Cell Death Dis.* 2021;12(3):240.

56. Chen A, et al. Chitinase-3-like 1 protein complexes modulate macrophage-mediated immune suppression in glioblastoma. *J Clin Invest.* 2021;131(16).

57. Kwon AHK, Liddelow SA. Astrocytes have a license to kill inflammatory T cells. *Immunity.* 2021;54(4):614-6.

58. Filippi M, et al. Identifying Progression in Multiple Sclerosis: New Perspectives. *Ann Neurol.* 2020; 88(3):438-452.

59. Reich DS, et al. Multiple Sclerosis. *N Engl J Med.* 2018;378(2):169-80.

60. Kang Z, et al. Astrocyte-restricted ablation of interleukin-17-induced Act1-mediated signaling ameliorates autoimmune encephalomyelitis. *Immunity.* 2010;32(3):414-25.

61. Yan Y, et al. CNS-specific therapy for ongoing EAE by silencing IL-17 pathway in astrocytes. *Mol Ther.* 2012;20(7):1338-48.

62. Mayo L, et al. Regulation of astrocyte activation by glycolipids drives chronic CNS inflammation. *Nat Med.* 2014;20(10):1147-56.

63. Wheeler MA, et al. Environmental Control of Astrocyte Pathogenic Activities in CNS Inflammation. *Cell.* 2019;176(3):581-96 e18.

64. Chao CC, et al. Metabolic Control of Astrocyte Pathogenic Activity via cPLA2-MAVS. *Cell.* 2019;179(7):1483-98 e22.

65. Rothhammer V, et al. Type I interferons and microbial metabolites of tryptophan modulate astrocyte activity and central nervous system inflammation via the aryl hydrocarbon receptor. *Nat Med.* 2016;22(6):586-97.

66. Rothhammer V, et al. Microglial control of astrocytes in response to microbial metabolites. *Nature.* 2018;557(7707):724-8.

67. Singh A, Sen D. Therapeutic Value of Adeno Associated Virus as a Gene Therapy Vector for Parkinson's Disease - A Focused Review. *Curr Gene Ther.* 2016;16(4):278-86.

68. Abudayyeh OO, et al. RNA targeting with CRISPR-Cas13. *Nature.* 2017;550(7675):280-4.

69. Konermann S, et al. Transcriptome Engineering with RNA-Targeting Type VI-D CRISPR Effectors. *Cell.* 2018;173(3):665-76 e14.

70. Croxford JL, et al. Different therapeutic outcomes in experimental allergic encephalomyelitis dependent upon the mode of delivery of IL-10: a comparison of the effects of protein, adenoviral or retroviral IL-10 delivery into the central nervous system. *J Immunol.* 2001;166(6):4124-30.

71. Zolotukhin S, et al. Recombinant adeno-associated virus purification using novel methods improves infectious titer and yield. *Gene Ther.* 1999;6(6):973-85.

72. Gray SJ, et al. Production of recombinant adeno-associated viral vectors and use in in vitro and in vivo administration. *Curr Protoc Neurosci.* 2011;Chapter 4:Unit 4 17.

73. Prah J, et al. A novel serum free primary astrocyte culture method that mimic quiescent astrocyte phenotype. *J Neurosci Methods.* 2019;320:50-63.

74. Butovsky O, et al. Identification of a unique TGF-beta-dependent molecular and functional signature in microglia. *Nat Neurosci.* 2014;17(1):131-43.

75. Najm FJ, et al. Transcription factor-mediated reprogramming of fibroblasts to expandable, myelinogenic oligodendrocyte progenitor cells. *Nat Biotechnol.* 2013;31(5):426-33.

Figure Legends

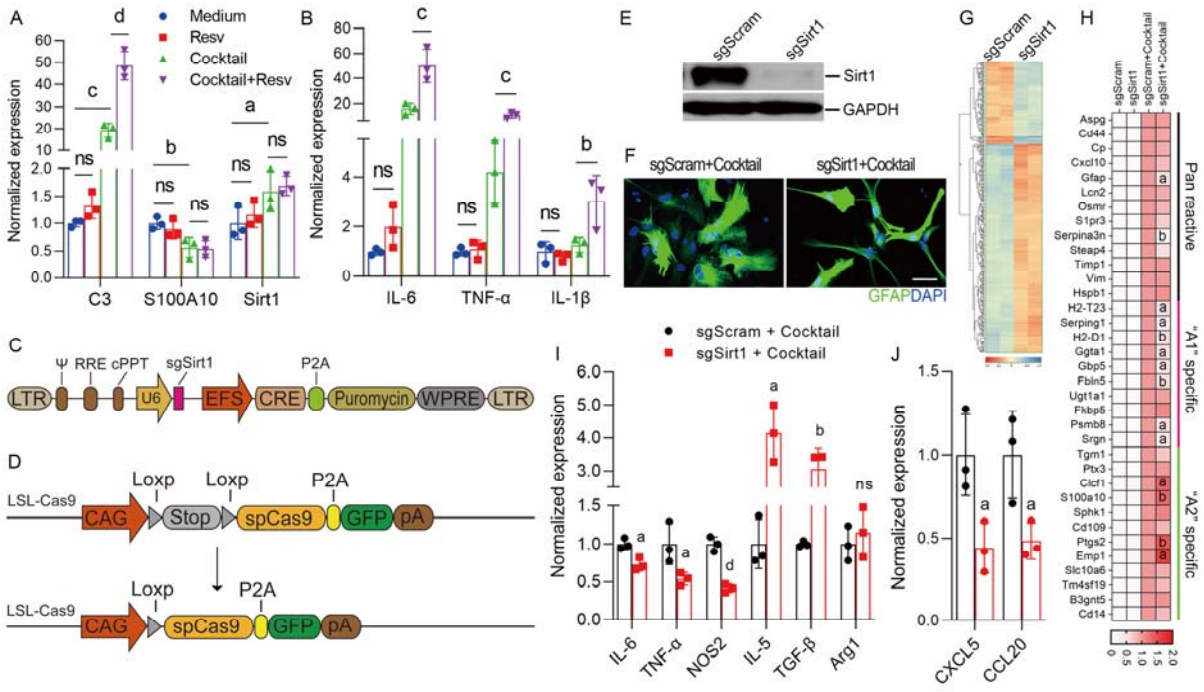

Figure 1. Inactivation of SIRT1 promoted anti-inflammatory astrocytes. (A-B) Primary astrocytes were isolated from naïve newborn C57BL/6 mice at P2, treated with resveratrol (Resv) or DMSO for 24 h, and then stimulated with a cocktail (C1q, TNF, IL-1α) for another 24 h. Expression of representative A1/A2 astrocyte markers (**A**) and proinflammatory cytokines (**B**) was determined by RT-PCR. n = 3 per group, one-way ANOVA. **(C-G)** Primary astrocytes isolated from LSL-Cas9 mice (**D**) were infected with lentivirus carrying *Cre* with sgSirt1 or sgScram (**C**). Forty-eight hours after infection, cells were selected with puromycin for 3 days, and knockout efficiency was analyzed by Western blot (**E**). sgSirt1- and sgScram-treated astrocytes were stimulated with the cocktail for 24 h and assayed by immunostaining for their morphology (**F**), by microarray for the RNA expression profiles (G), and by RT-PCR for the expression of neurotoxic ("A1"), neuroprotective ("A2") and pan-reactive astrocyte markers (8) (**H**), pro- or anti-inflammatory molecules (**I**), and chemokines (**J**). n = 3 per group, unpaired two-tailed t test. All

results are expressed as means ± SD, a = $p < 0.05$, b = $p < 0.01$, c = $p < 0.001$, d = $p < 0.0001$, ns = not statistically significant. One representative of 3 experiments is shown.

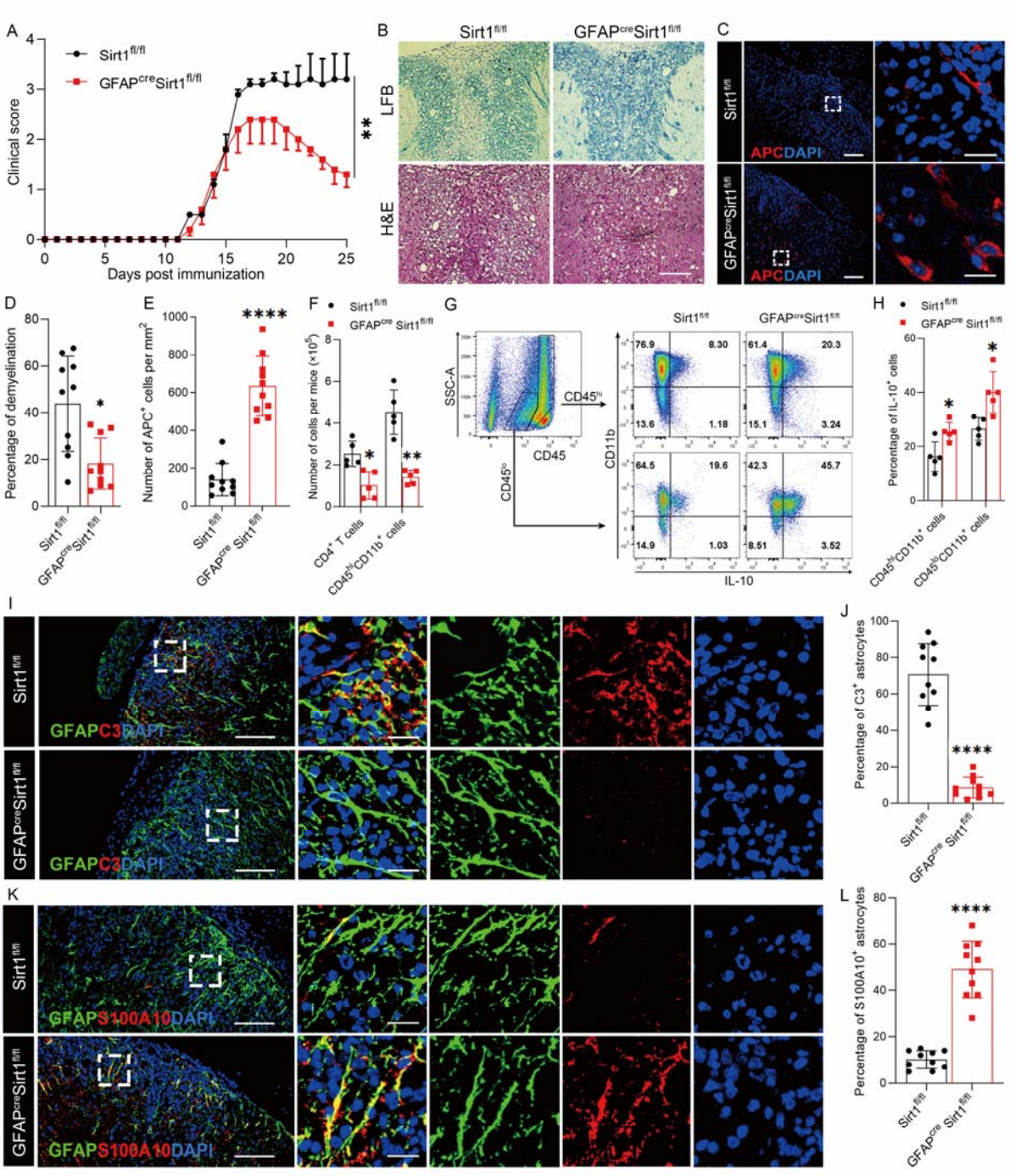

Figure 2. Astrocyte-specific knockout of *Sirt1* suppressed EAE progression. EAE was induced in GFAP^{cre}*Sirt1*$^{fl/fl}$ or *Sirt1*$^{fl/fl}$ control mice by MOG_{35-55} peptide in CFA and pertussis toxin. **(A)** Clinical signs were scored by two researchers in a blinded manner following a 0-5 scale. n = 5 mice each group, two-way repeated measures ANOVA. Results are expressed as mean ± SEM. Mice were sacrificed at day 25 p.i. **(B)** Representative LFB and H&E stained images of spinal cord from EAE mice. Scale bar, 50 μm. **(C)** Immunofluorescence staining of spinal cord from EAE mice with APC (CC1), a marker for newly formed oligodendrocytes. Scale bar: 100 μm. The right panel is the larger magnification of the inserts shown in the left panel, scale bar: 20 μm. **(D-E)** Statistical analysis of LFB (**D**) and APC (**E**) staining results. n=5 mice per group, unpaired two-tailed t test. **(F)** The total number of $CD4^+$ T cells and myeloid cells ($CD45^{hi}CD11b^+$) from the CNS of GFAP^{cre}*Sirt1*$^{fl/fl}$ or *Sirt1*$^{fl/fl}$ mice were analyzed by flow cytometry. **(G)** The expression of IL-10 in $CD45^{hi}$ (myeloid) and $CD45^{low}$ (microglia) cells from GFAP^{cre}*Sirt1*$^{fl/fl}$ or *Sirt1*$^{fl/fl}$ EAE mice was analyzed by flow cytometry. **(H)** Statistical analysis of **(G)**. n=5 mice per group, unpaired two-tailed t test. **(I-L)** Spinal cords were stained with GFAP and C3, a representative of neurotoxic astrocytes (**I**), as well as GFAP and S100A10, a representative of anti-inflammatory astrocytes (**K**). Scale bar: 100 μm. The right panels of **I** and **K** are the larger magnification of the inserts shown in the left panel. The percentages of $C3^+$ (**J**) and $S100A10^+$ (**L**) astrocytes were quantified. n = 5 mice per group. D,E,F,H,J, and L are expressed as means ± SD, unpaired two-tailed t test. *p < 0.05, **p < 0.01, ****p < 0.0001. One representative of 3 experiments is shown.

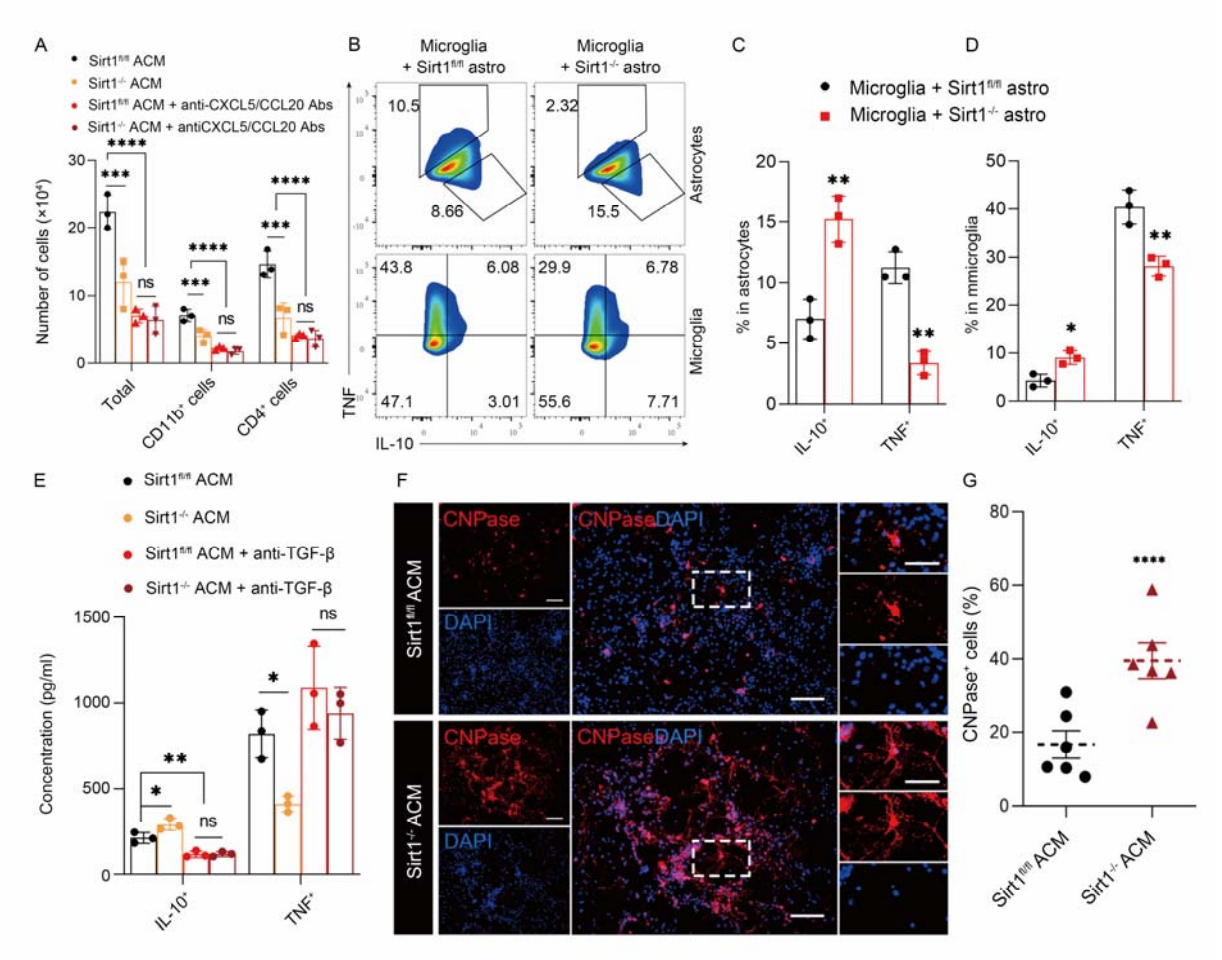

Figure 3. Astrocyte-specific *Sirt1*$^{-/-}$ reduced migration and inflammation of immune cells and enhanced OPC differentiation. Astrocytes isolated from brains of newborn GFAP^{cre}*Sirt1*$^{fl/fl}$ or *Sirt1*$^{fl/fl}$ mice were stimulated with cocktail for 24 h, washed, and cultured in fresh medium. These astrocytes were cultured for an additional 24 h to collect supernatant (astrocyte-conditioned medium; ACM). **(A)** Splenocytes of WT EAE mice were harvested at day 12 p.i., and cultured with ACMs from *Sirt1*$^{-/-}$ or WT astrocytes using a transwell cell culture insert. Cells in the bottom chamber were harvested 2 h later, and migration of CD4$^+$ T cells and CD11b$^+$ cells was analyzed by flow cytometry. n = 3 samples per group, one-way ANOVA. **(B)** Microglia were isolated from brains of newborn WT mice, pre-activated with LPS for 18 h, and co-cultured with cocktail-stimulated *Sirt1*$^{-/-}$ or WT astrocytes for 24 h. Production of TNF and IL-10 by astrocytes and microglia was analyzed by flow cytometry. **(C-D)** Statistical analysis of (**B**).

n = 3 samples per group, unpaired two-tailed t test. **(E)** LPS-stimulated microglia were incubated in *Sirt1*$^{-/-}$ or control ACMs with or without anti-TGF-β neutralizing antibody for 24 h, then washed and cultured in fresh medium for an additional 24 h, after which the concentrations of TNF and IL-10 in culture supernatants were measured by ELISA. n = 3 samples per group, one-way ANOVA. **(F-G)** OPCs were generated from brains of newborn WT mice, cultured in differentiation medium that was supplemented with ACMs of cocktail-stimulated *Sirt1*$^{-/-}$ or WT astrocytes for 8 days, and stained for MBP. Data were statistically analyzed by unpaired two-tailed t test (n=3 samples per group). Scale bar: 50 μm. The right panel in **F** is the larger magnification of the inserts shown in the middle panel, scale bar: 25 μm. All results are expressed as mean ± SD, * P<0.05, ** P<0.01, *** P<0.001, **** P<0.0001. One representative of 3 experiments is shown.

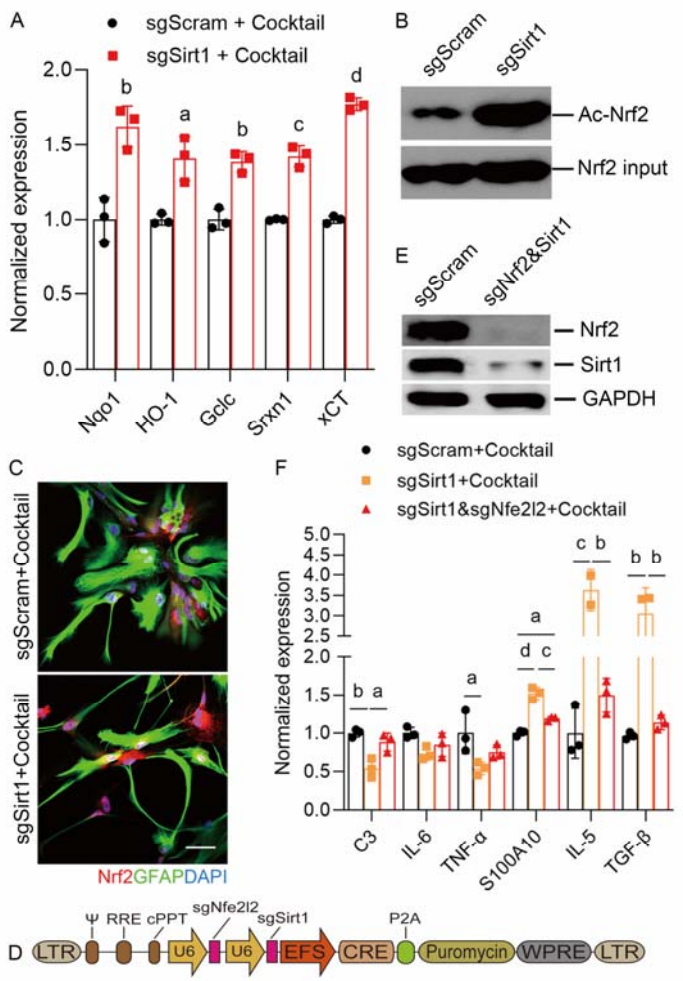

Figure 4. SIRT1 enhanced A1 astrocytes by inhibiting the activity of NRF2. mRNA was extracted from sgSirt1- or sgScram-treated astrocytes after stimulation with the cocktail containing C1q, IL-1α and TNF for 24 h and used for RT-PCR analysis. **(A)** The expression of NRF2 target genes by RT-PCR. n=3 per group, unpaired two-tailed t test. **(B)** IP analysis of NRF2 acetylation in sgSirt1 and sgScram treated astrocytes. **(C)** Immunostaining of NRF2 in astrocytes. Scale bar: 50 μm. **(D-F)** Primary astrocytes were transduced with sgSirt1, sgSirt1& sgNfe2l2, or sgScram vectors, then stimulated with the cocktail for 24 h. **(D)** Structure of lentivirus carrying sgSirt1 and sgNfe2l2. **(E)** Western-blot verification of knockout of *Sirt1* and *Nfe2l2*. **(F)** Expression of certain reactive astrocytes markers and cytokines was determined by

RT-PCR. n=3 per group, one-way ANOVA. All results are expressed as mean ± SD, a: $p<0.05$; b: $p<0.01$; c: $p < 0.001$; d: $p<0.0001$. One representative of 3 experiments is shown.

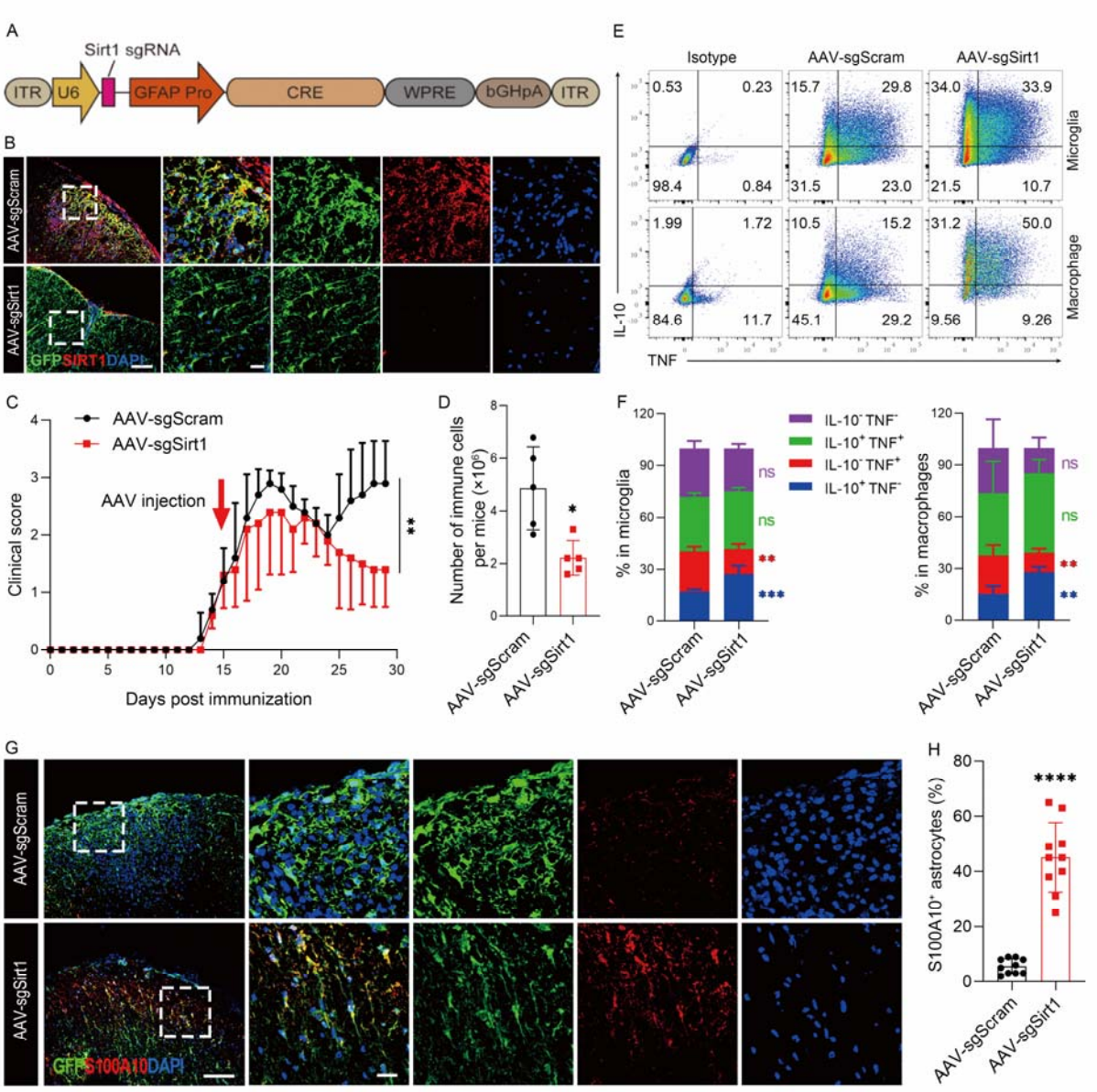

Figure 5. CRISPR/Cas9-mediated astrocyte-specific *Sirt1* knockout effectively alleviated ongoing EAE. (A) Structure of AAV plasmid for *Sirt1* knockout *in vivo*. **(B-H)** EAE was induced in LSL-Cas9 mice (C57BL/6 background) by MOG_{35-55} peptide in CFA and pertussis toxin. AAV carrying *Sirt1* sgRNA

or scramble sgRNA was injected through the tail vein at day 15 p.i. Mice were sacrificed at day 30 p.i. and brain, spinal cord, and spleen were harvested. **(B)** Knockout efficiency of *Sirt1* in astrocytes was determined by immunostaining of lumbar spinal cord. Scale bar: 100 μm. The right panels are the larger magnification of the inserts shown in the left panel, scale bar: 20 μm. **(C)** EAE score of AAV-sgSirt1 and AAV-sgScram injected mice. n=5 mice for AAV-sgSirt1 group and n=8 mice for AAV-sgScram group, two-way repeated measures ANOVA. **(D)** Statistical analysis of the numbers of MNCs in the CNS of mice with EAE. **(E)** Flow cytometry analysis of percentages of different phenotypes of microglia ($CD45^{lo}$ $CD11^{+}$) and macrophages ($CD45^{hi}$ $CD11^{+}$) in the CNS of mice with EAE. **(F)** Statistical analysis of (**E**). **(G)** Spinal cords from AAV-sgSirt1- or AAV-sgScram-injected mice with EAE were co-stained with GFP (astrocytes infected by AAV) and S100A10. Scale bar: 100 μm. The right panels are the larger magnification of the inserts shown in the left panel, scale bar: 20 μm. **(H)** Statistical analysis of percentages of $S100A10^{+}$ astrocytes. D-H, n=5 mice per group, unpaired two-tailed t test. All results are expressed as means ± SD, *$p < 0.05$, **$p < 0.01$, ***$p < 0.001$, ****$p < 0.0001$. One representative of 2 experiments is shown.

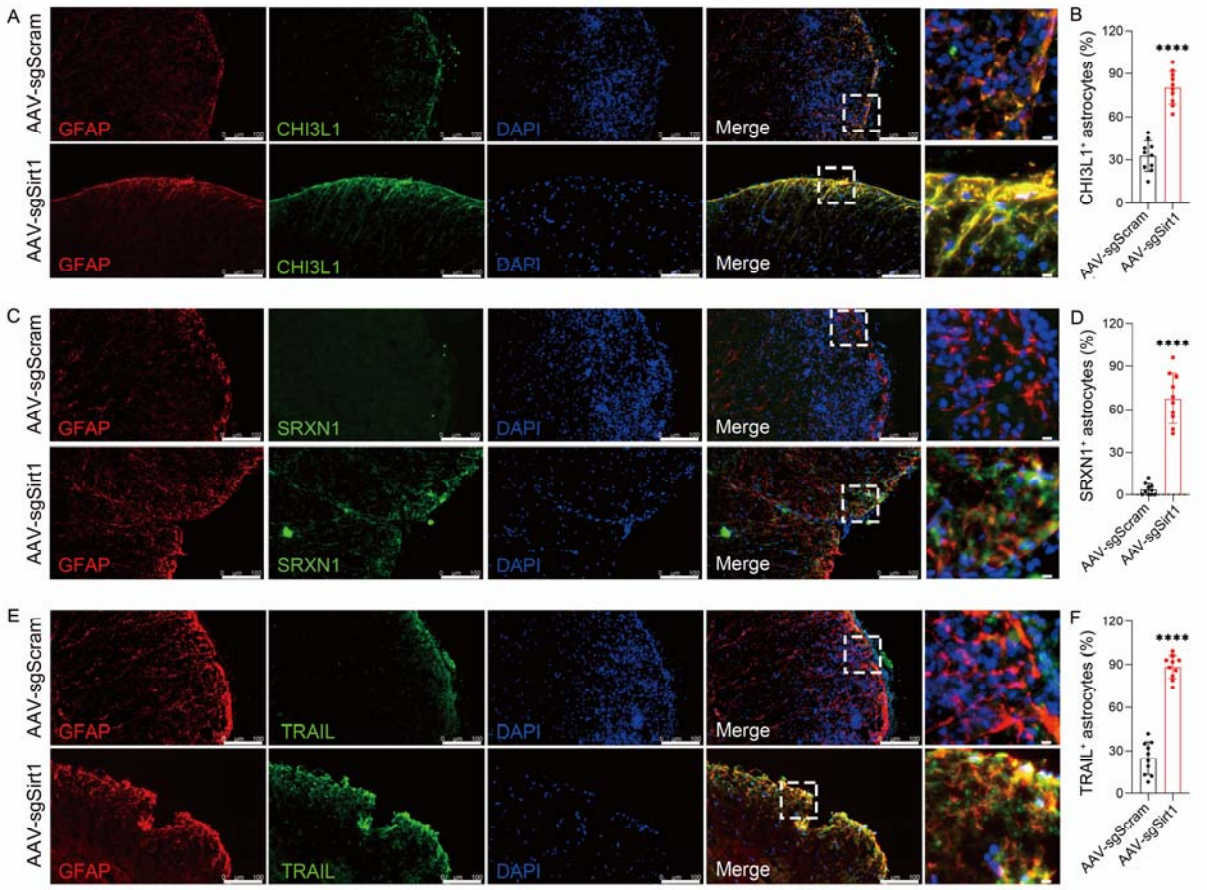

Figure 6. Immunostaining analysis of astrocytes in astrocyte-specific *Sirt1* knockout and WT EAE mice. Spinal cords from AAV-sgSirt1- or AAV-sgScram-injected mice with EAE were co-stained for GFAP and CHI3L1 (A,B), SRXN1 (C,D), Trail (E,F). A,C,E: scale bar: 100 μm. The right panels are the larger magnification of the inserts shown in the left panel, scale bar: 100 μm. B,D,F: n=5 mice per group, unpaired two-tailed t test. All results are expressed as means ± SD, *p < 0.05, **p < 0.01, ***p < 0.001, ****p < 0.0001. One representative of 2 experiments is shown.

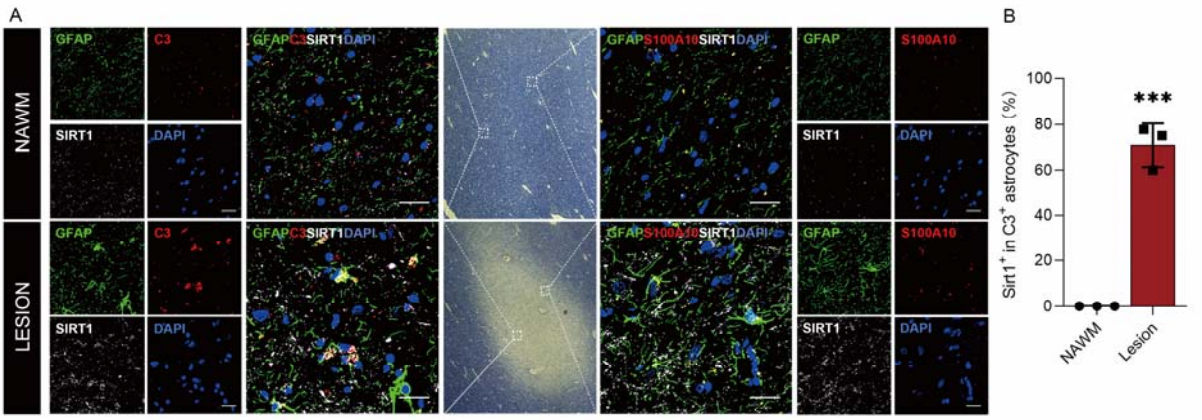

Figure 7. SIRT1 is highly expressed in A1 astrocytes in lesions of MS patients. (A) Brain tissues from MS patients were co-immunostained for GFAP, SIRT1, and DAPI with C3 or S100A10; and NAWM served as control. The left and right panels are the larger magnification of the inserts shown in the middle panel, scale bar: 100 μm. **(B)** Statistical analysis. For quantification, lesion tissues from the brain of three MS patients were examined. Nine sections (three per lesion) were randomly selected and quantitated. The number of stained cells per section was counted under ×40 magnification. Data are expressed as mean ± SD; unpaired two-tailed t test; ***$p < 0.001$.